

## STRUCTURAL INTEGRITY-IN UNCONSTRAINED DENSIFICATION OF PARTIALLY DELIGNIFIED POPLAR

ABDÜLHALİM BEŞPARMAK, HASAN ÖZGÜR IMIRZI  
GAZI UNİVERSİTESİ  
TÜRKİYE

RECEIVED DECEMBER 2025

### ABSTRACT

In this study, the effects of a chemical-mechanical modification system on low-density poplar (*Populus tremula* L.) wood were investigated without external confinement. Wood samples were initially treated with an alkali-sulphite solution (2.5 M NaOH, 0.4 M Na<sub>2</sub>SO<sub>3</sub> for 7 h) to induce partial delignification, after which they were densified at 100°C under 5 MPa pressure. Following this process, a significant increase in density to 1.22 g/cm<sup>3</sup> (+172.6%) was recorded. Mechanical evaluations indicated substantial enhancements; specifically, Brinell hardness, bending strength (MOR), and modulus of elasticity (MOE) were improved by 346.3%, 67.4%, and 78.3%, respectively, confirming the successful consolidation of the cellulose network. However, a trade-off was revealed by microscopic analysis, and two distinct failure mechanisms were identified. First, large cracks (~150 µm) were formed in the core due to diffusion limitations that prevented full chemical penetration. Second, widespread micro-cracks (~4 µm) were triggered in the densified shell by the Poisson effect due to the lack of lateral confinement. These results suggest that while hardness is significantly improved by unconstrained densification, compressive performance is compromised by the resulting defects. While the modification was intentionally applied to 35 mm thick lumber to reveal diffusion limitations and Poisson-induced defects under unconstrained conditions, small, defect-free specimens were subsequently selected for mechanical testing to isolate and characterize the intrinsic properties of the successfully modified regions near the surface.

**KEYWORDS:** Partial delignification, unconstrained densification, micro-cracks, Brinell hardness, compressive strength, failure mechanisms.

### INTRODUCTION

Poplar wood is widely recognized as a strategic biomass resource for industrial use, owing to its extensive plantation areas and rapid growth cycles (Balatinecz & Kretschmann 2001).

However, its utilization in structural engineering is severely limited by a low density ( $<0.45 \text{ g/cm}^3$ ) and the large proportion of lumen voids within its anatomy. As highlighted in recent studies (Cheng et al. 2022; Bytner et al. 2021), the application of poplar in high-value products is hindered by native deficiencies such as a loose structure, high hygroscopicity, and poor dimensional stability, which necessitates the development of effective modification strategies. These anatomical characteristics directly restrict critical mechanical properties, specifically the modulus of elasticity (MOE), surface hardness, and specific strength (Chen et al. 2020; Sandberg et al. 2013).

In prior research focusing on poplar (*Populus nigra* L.), it was documented that mechanical properties, such as bending strength and modulus of elasticity, are substantially augmented by densification, with increases of up to 444% being reported (Ülker & Burdurlu 2016). However, while mechanical performance is enhanced through the reduction of porosity, the industrial scalability of traditional thermo-hydro-mechanical (THM) processes is restricted. Specifically, the widespread application of these methods is often limited by the occurrence of cell wall fractures and moisture-induced 'set-recovery' phenomena (Navi & Heger 2004; Kutnar & Kamke 2012; Morsing 2000).

To address the inherent limitations of purely mechanical densification, attention has been increasingly directed toward chemical pretreatments. Through the removal of matrix polymers, the cell wall structure is softened and nano-porosity is introduced (Song et al. 2018; Zhu et al. 2016). A reduction in the glass transition temperature ( $T_g$ ) is thereby achieved, a critical modification that enables cellulose microfibrils to undergo folding without fracture during pressing—a phenomenon described as 'super-flexibility' (Frey et al. 2019). Following compression, substantial stiffness is developed in the material via a 'molecular locking' mechanism, which is sustained by the formation of dense hydrogen bonds and Van der Waals forces at the nanoscale (Chen et al. 2020).

While idealized outcomes of delignification-based densification using confined moulds have been emphasized in the majority of literature (Tenorio et al. 2021), the Poisson effect - a distinct mechanical challenge introduced by unconstrained pressing—has been largely overlooked. Despite this oversight, unconstrained pressing is retained as the primary technology for cost-effective, high-volume production, mirroring the conditions of industrial continuous presses. Under uniaxial compression, lateral expansion is exhibited by the naturally anisotropic wood structure. Consequently, high tensile and shear stresses are induced within the tissue, being specifically concentrated in anatomically weak regions such as the ray parenchyma (Navi & Sandberg 2012; Bodig & Jayne 1982). It is observed that increased brittleness and unstable crack propagation are precipitated by this structural degradation, as evidenced by the stagnation of fracture toughness values despite significant density gains (Yoshihara & Nobusue 2008).

Process parameters, specifically pressing temperature and compression ratio, are recognized as decisive factors in the formation of the vertical density profile, which is directly correlated with surface hardness and overall mechanical performance (Zhou et al. 2023). This relationship is strongly supported by Zhou et al. (2019), who demonstrated that in the thermo-hydro-mechanical (THM) surface densification of poplar solid wood, specific vertical density profile indices—namely peak density (PD) and the thickness of the densified zone (DTh)—are the most relevant determinants of surface hardness. Their study revealed that when the PD and

DTh are greater, the surface hardness is correspondingly enhanced. Furthermore, they established that while higher compressing temperatures (e.g., 180°C) yield a greater peak density and higher surface hardness, excessive heat causes the peak density to shift deeper into the wood core, highlighting the necessity of parameter optimization to keep the hardest zone near the surface. A strong positive correlation between the densification ratio and Brinell hardness was documented in surface-densified wood, where it was highlighted that mechanical resistance is significantly enhanced even by moderate compression of the surface layers (Rautkari et al. 2009). While wood density is identified as the governing parameter for the resulting material properties (Wang et al. 2020), dimensional stability is persistently threatened by the 'set-recovery' phenomenon. This instability arises when stored elastic energy within the cell wall is not fully dissipated. Upon wetting, it has been observed that up to 60% of the deformation in densified wood can be recovered (Laine et al. 2016). Such a 'shape memory' effect is attributed to the retention of elastic strain energy within the lignin and microfibrillar structures (Navi & Heger 2004).

The efficacy of partial delignification on bulk natural wood has been well-documented in recent literature (Song et al. 2018; Frey et al. 2019); however, the diffusion behaviour and structural integrity of thicker cross-sections - such as 35 mm poplar lumber-subjected to unconstrained pressing remain underexplored. In particular, the interaction between diffusion limitations and the Poisson effect during industrial pressing has not been adequately defined. Consequently, the structural integrity trade-offs involved in scaling up the partial delignification and densification process without lateral confinement are characterized in this study to support industrial implementation.

## MATERIAL AND METHODS

Sapwood of poplar (*Populus tremula* L.) was procured from commercial plantations in Ankara, Turkey, and subsequently machined into defect-free specimens with dimensions of 35 × 90 × 150 mm (R × T × L). Before treatment, the samples were stabilized in a climate chamber controlled at 20°C and 65% relative humidity (RH) until an equilibrium moisture content (EMC) of approximately 12% was attained.

### **Chemical pretreatment (partial delignification)**

Partial delignification was carried out using an alkali-sulphite system to enhance cell wall viscoelasticity. Samples were treated with an aqueous solution of 2.5 M NaOH and 0.4 M Na<sub>2</sub>SO<sub>3</sub> at boiling temperature (100°C) for 7 h, in accordance with the protocol described by Song et al. (2018). The specific reaction parameters (concentration and duration) were replicated directly from this established methodology.

### **Unconstrained thermo-mechanical densification**

The densification process was governed by displacement control, employing metal stops to fix the final target thickness at 12 mm. While vertical displacement was restricted by these stops, lateral restraint was intentionally omitted, thereby permitting free expansion in the tangential direction. A specific pressure of 5 MPa was applied until the platens were seated

against the mechanical stops, after which the position was maintained throughout the thermal treatment. This approach was selected to guarantee a uniform compression ratio across all samples, independent of minor variations in initial density.

## Characterization and testing

### *Compressive strength*

Air-dry density was determined according to TS EN 323 based on mass and volume measurements. Compressive strength parallel to the grain was determined in accordance with the ASTM D4761 standard (Fig. 2b), and the results were calculated using Eq. 1. The specimens were prepared with dimensions of 6 x 6 x 9 mm (T x R x L) and conditioned to an air-dry moisture content. Following the drying process, the dimensions were measured using a calliper with a precision of 0.01 mm. The compressive load was applied parallel to the grain direction:

$$\sigma_{(comp)} = F_{max}/A \quad (\text{N/mm}^2) \quad (1)$$

where:  $\sigma_{(comp)}$  - compressive strength (N/mm<sup>2</sup>),  $F_{max}$  - maximum force at compressive (N),  $A$  – cross-sectional area (mm<sup>2</sup>).

### *Modulus of rupture and modulus of elasticity in flexural strength*

Modulus of rupture (MOR) and modulus of elasticity (MOE) were determined via three-point static bending tests (Fig. 1a). Before testing, specimens with dimensions of 120 x 7 x 6 mm (L x T x R) were conditioned to an air-dry state. An Instron 5869 universal testing machine was employed with a span length of 90 mm. The load was applied at mid-span, perpendicular to the growth rings, until failure occurred. A constant crosshead speed of 5 mm/min was maintained to ensure the maximum load was reached within the time frame specified by the standard. The MOR values were calculated using Eq. 2, and the MOE values were calculated using Eq. 3, based on an average of 8 replicates per sample set:

$$\sigma_{(MOR)} = 3 \cdot F_{max} \cdot L_s / 2 \cdot b \cdot h^2 \quad (\text{N/mm}^2) \quad (2)$$

where:  $\sigma_{(MOR)}$  – modulus of rupture (MOR),  $F_{max}$  - maximum force at fracture (N),  $L_s$  - distance between two supports (mm),  $b$  - width of the sample (mm),  $h$  - thickness of the sample (mm).

$$\sigma_{(MOE)} = (I^3 / 4 \cdot b \cdot t^3) \cdot K \quad (\text{N/mm}^2) \quad (3)$$

where:  $\sigma_{(MOE)}$  – modulus of elasticity (MOE),  $I$  - distance between two supports (mm),  $b$  - width of the test sample (mm),  $h$  - thickness of the test sample (mm),  $K$  - slope of the load deformation curve between 20% and 40% of the maximum force.

### *Brinell hardness test*

Brinell hardness tests were conducted in accordance with the TS EN 1534 (Fig. 1c). A total of 12 specimens were utilized, consisting of six samples with dimensions of 20 x 20 x 20 mm

and six samples measuring 20 x 20 mm. A static load of 1000 N was applied vertically to the wood surface using a 5 mm diameter ball indenter. The diameter of the resulting indentation was determined by averaging measurements taken across two orthogonal axes. Subsequently, the Brinell hardness values were calculated by substituting these measurements into Eq. 4:

$$HB = 2 \cdot F / g \cdot \pi \cdot D [(D - \sqrt{D^2 - d^2})] \quad (4)$$

where: HB- Brinell hardness (N/mm<sup>2</sup>), g - gravitational force (m/s<sup>2</sup>),  $\pi$  – pi number, F - max applied force (N), D - diameter of the ball (mm), d - diameter of deformation residue (mm).

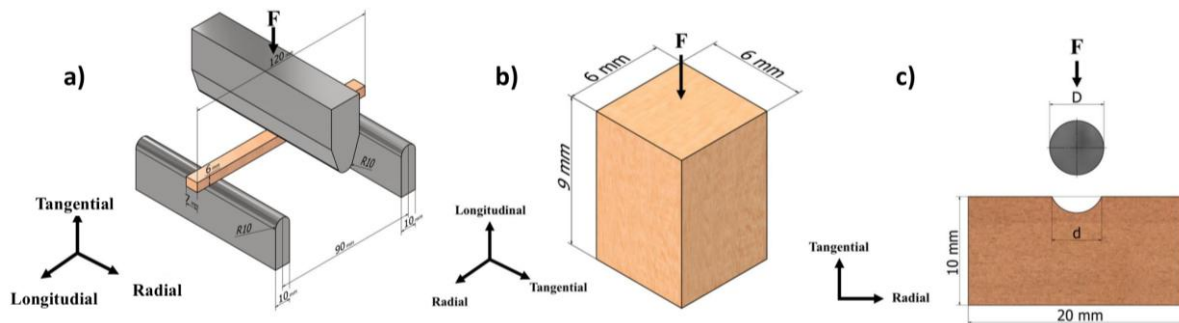


Fig. 1: Mechanical test specimen dimensions: a) three-pointed bending strength test, b) parallel to grain compressive strength test, c) Brinell hardness test.

### Morphological analysis

Structural changes, lumen collapse, and defect formation were analysed using a Stereo Microscope (Leica M205 C) and a Scanning electron microscope (SEM) (JEOL JSM 6060 LV) to detect macro- and micro-cracks.

### Statistical analysis

Statistical analysis was performed to evaluate the differences in mechanical properties (Brinell hardness, compressive strength, flexural strength, and flexural modulus) between control and densified samples. One-way analysis of variance (ANOVA) was utilized to analyse the data. In cases where significant differences were detected by ANOVA, the Least significant difference (LSD) post-hoc test was applied to determine specific differences between the group means. For all statistical evaluations, the significance level was set at  $p < 0.05$ . The results are presented as mean values  $\pm$  standard deviation. Statistical analyses were performed using Python programming language (v3.x) with SciPy and NumPy libraries.

## RESULTS AND DISCUSSION

By strictly adopting the delignification protocol optimized by Song et al. (2018) (2.5 M NaOH, 0.4 M Na<sub>2</sub>SO<sub>3</sub>, 7 h), the targeted softening behaviour of the cell wall components was successfully achieved. Indeed, while control specimens exhibited brittle fracture under 5 MPa pressure, the treated samples underwent extensive plastic deformation without disintegration. This behaviour serves as the primary macroscopic indicator that the alkali-sulphite protocol

effectively lowered the glass transition temperature ( $T_g$ ) and induced the necessary cell wall buckling, a mechanism similar to the thermal softening effects described by Cheng et al. (2022) for heat-treated densified poplar. Following this modification, the unconstrained densification process resulted in a dramatic increase in air-dry density, rising from an average of 0.44 g/cm<sup>3</sup> to 1.22 g/cm<sup>3</sup>. This represents an approximate 172.6% improvement, confirming the effective collapse of the cellular structure and the reduction of void volume within the wood matrix. These density gains are consistent with the findings of Ülker and Burdurlu (2016), who reported that significant density increases in *Populus nigra* L. are the fundamental driver for mechanical enhancement. Furthermore, Chu et al. (2023) highlighted that such removal of matrix polymers facilitates a transition from brittle failure to ductile compaction, which explains how our samples achieved such high densification ratios (1.22 g/cm<sup>3</sup>) even under unconstrained conditions. Consequently, this structural evolution led to substantial enhancements in static mechanical properties (Tab. 1).

Tab. 1: Mechanical properties of control and densified poplar wood.

Properties	Control samples	Densified samples	F-value	p-value	LSD (0.05)
HB (N/mm <sup>2</sup> )	32.75 ± 1.83	146.17 ± 11.42	576.75	< 0.001*	10.52
$\sigma_{(comp)}$ (N/mm <sup>2</sup> )	33.47 ± 10.43	37.11 ± 9.86	0.51	0.485ns	10.88
$\sigma_{(MOR)}$ (N/mm <sup>2</sup> )	71.54 ± 3.54	119.76 ± 14.69	81.42	< 0.001*	11.46
$\sigma_{(MOE)}$ (N/mm <sup>2</sup> )	6930.14 ± 1365.94	12356.05 ± 2633.94	26.75	< 0.001*	2249.91

\* Significant at  $p < 0.05$  level; ns: not significant. Values are presented as mean ± standard deviation.

### Modulus of rupture (MOR) and modulus of elasticity (MOE)

The results for bending properties are summarized in Fig. 2a, revealing a significant structural enhancement with a 67.4% increase in MOR and a 78.3% increase in MOE. These findings validate the efficacy of the treatment and align with the strengthening trends reported for densified poplar species in the literature. For instance, Ülker and Burdurlu (2016) reported substantial improvements in the bending strength of *Populus nigra* L. through densification, attributing the gains to the increased biomass per unit volume. In our study, the MOR increase demonstrates that the unconstrained densified material can sustain significantly higher loads, a crucial requirement for structural applications. Furthermore, the high MOE value (12,356 N/mm<sup>2</sup>) indicates a major gain in stiffness. This is consistent with the findings of Li et al. (2021), who established a direct correlation between densification ratio and stiffness in engineered poplar products, as well as the theoretical premise of consolidated cellulose microfibrils and increased hydrogen bonding described by Chen et al. (2020). Similarly, Pelit et al. (2018) investigated the thermo-mechanical densification of black poplar (*Populus nigra* L.) and reported parallel increases in bending properties dependent on the compression ratio. Specifically, for black poplar samples densified at 100°C with a 50% compression ratio, they observed a 55% increase in MOR and a 42% increase in MOE compared to not-densified control samples. Furthermore, the maximum MOE value recorded for their densified black poplar was 12,220 N/mm<sup>2</sup>. This closely mirrors our finding of 12,356 N/mm<sup>2</sup>, strongly supporting the dramatic gains in structural stiffness achieved through the densification process.

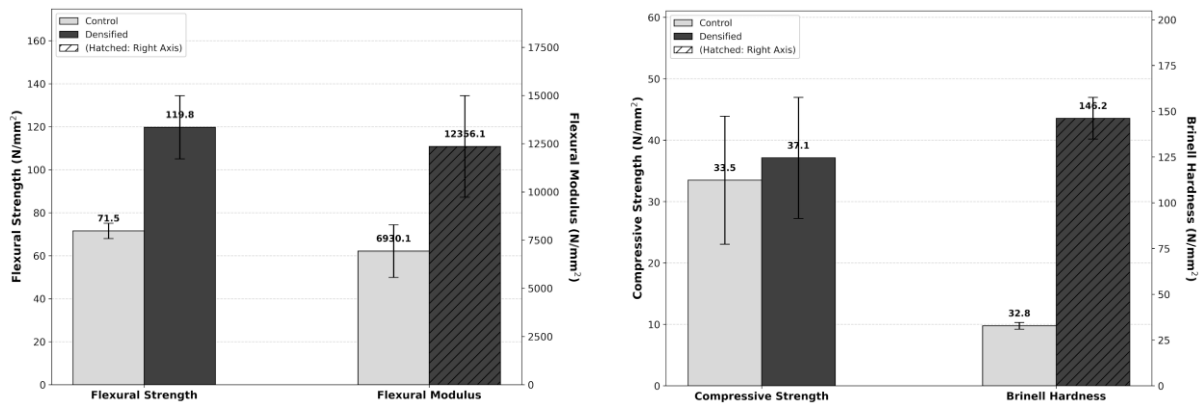


Fig. 2: Bending properties (a) and compressive strength and hardness (b) of control and densified poplar wood.

### Compressive strength and hardness

The vertical density profile observed in our samples, characterized by higher density at the surface layers, directly correlates with the substantial enhancement in mechanical properties. This observation aligns with Zhou et al. (2019), who identified that specific vertical density profile indices, particularly the peak density (PD) and the thickness of the densified zone (DTh), are the primary determinants of surface hardness in densified poplar. Specifically, Brinell hardness exhibited the most dramatic improvement, surging by 346.3% to 146.17 N/mm<sup>2</sup>, effectively elevating the poplar's surface hardness to a level comparable to high-density hardwoods. This improvement significantly outperforms the 108% increase in Janka hardness reported by Zhou et al. (2019) for poplar treated via thermo-hydro-mechanical (THM) densification without chemical pretreatment, highlighting the superior efficacy of the chemical modification employed in this study. This significant rise also aligns with Zhou et al. (2023), confirming that the density gradient formed during the unconstrained process governs indentation resistance.

Microscopic evaluations further support these gains, revealing that the improvement is driven by the extensive collapse of vessel elements and the reduction of void volume. Consistent with the mechanism described by Cheng et al. (2022), this compaction was facilitated by the 'super-flexibility' induced by the chemical pretreatment, which minimized cell wall fractures during pressing and created a highly integrated solid structure. In contrast, purely thermal softening as utilized by Zhou et al. (2019) relies heavily on higher compressing temperatures (e.g., 180°C) to plasticize the surface, which yielded lower densification ratios compared to the chemically assisted compression achieved here.

This structural consolidation also yielded a 10.9% increase in longitudinal compressive strength, reaching 37.11 N/mm<sup>2</sup> (Fig. 2b), a trend supported by Li et al. (2021) and Ülker and Burdurlu (2016) regarding the load-bearing capacity of densified wood. However, this increase was notably limited compared to the improvements in hardness. While the pretreatment prevented brittle failure, the removal of the lignin matrix (Wang et al. 2021) and the lack of lateral support in the unconstrained densification method predisposed fibres to instability. Unlike the isostatic pressing described by Yu et al. (2017), the empty lumens in our study allowed internal stresses generated by the Poisson effect to develop into micro-cracks, acting

as stress concentration points that triggered premature failure. This contrasts with Kuai et al. (2022), who achieved an extraordinary compressive strength of 228.5 MPa by impregnating delignified poplar wood with sodium silicate, where inorganic fillers provided support to cell lumens and prevented buckling. Furthermore, Lykidis et al. (2020) noted that impregnation with matrices like melamine formaldehyde enhances stability and reduces set-recovery. Therefore, despite the high hardness achieved in this study, further elevating compressive strength requires integrating impregnation matrices as suggested by Kuai et al. (2022) and Lykidis et al. (2020), or employing laterally confined pressing techniques as proposed by Yu et al. (2017).

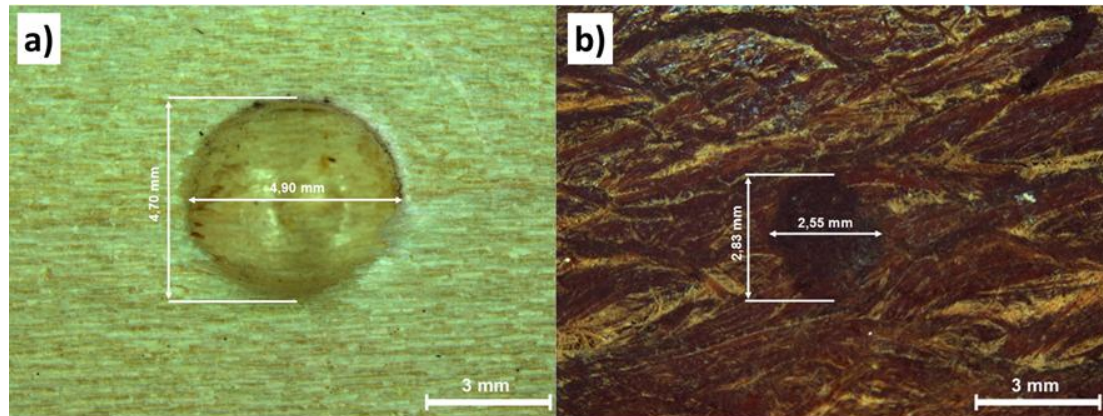


Fig. 3: Indentation diameters after Brinell hardness test: a) natural poplar, b) densified poplar.

### Morphological findings: Dual mechanism of defect formation

Microscopic analysis revealed that the property gains are driven by the extensive collapse of vessel elements and the reduction of lumen void volume. Cheng et al. (2022) described a similar mechanism in heat-treated densified poplar, where cell wall collapse provided a compact surface ideal for machining and coating. Additionally, the study by Li et al. (2021) on the engineering application potential of densified poplar emphasized that this cellular compaction is directly responsible for the increased nail-holding power and shear strength. In our samples, the chemical pretreatment likely facilitated this compaction at lower pressures compared to purely thermal modification, as the removal of lignin reduced the cell wall's resistance to buckling. Detailed stereo microscope and SEM analyses provided crucial evidence regarding the limitations of the process, revealing distinct failure mechanisms in different regions of the wood cross-section, as illustrated in Fig. 4.

### Diffusion limitation and core macro-cracks (~150 $\mu\text{m}$ )

Stereo microscopic examination of the cross-sections (Fig. 4b) revealed a significant gradient in modification. Microscopic analysis of the cross-sections (Fig. 4b) showed a clear modification gradient. Even though the 7-hour protocol works well in other studies (Song et al. 2018), we found diffusion limits in our setup. Applying standard boiling parameters to 35 mm thick lumber failed to achieve full chemical penetration. The lignin matrix in the central zones remained rigid and intact. As a result, the core fibres did not soften enough during hot-pressing (100°C) to deform plastically or form hydrogen bonds.

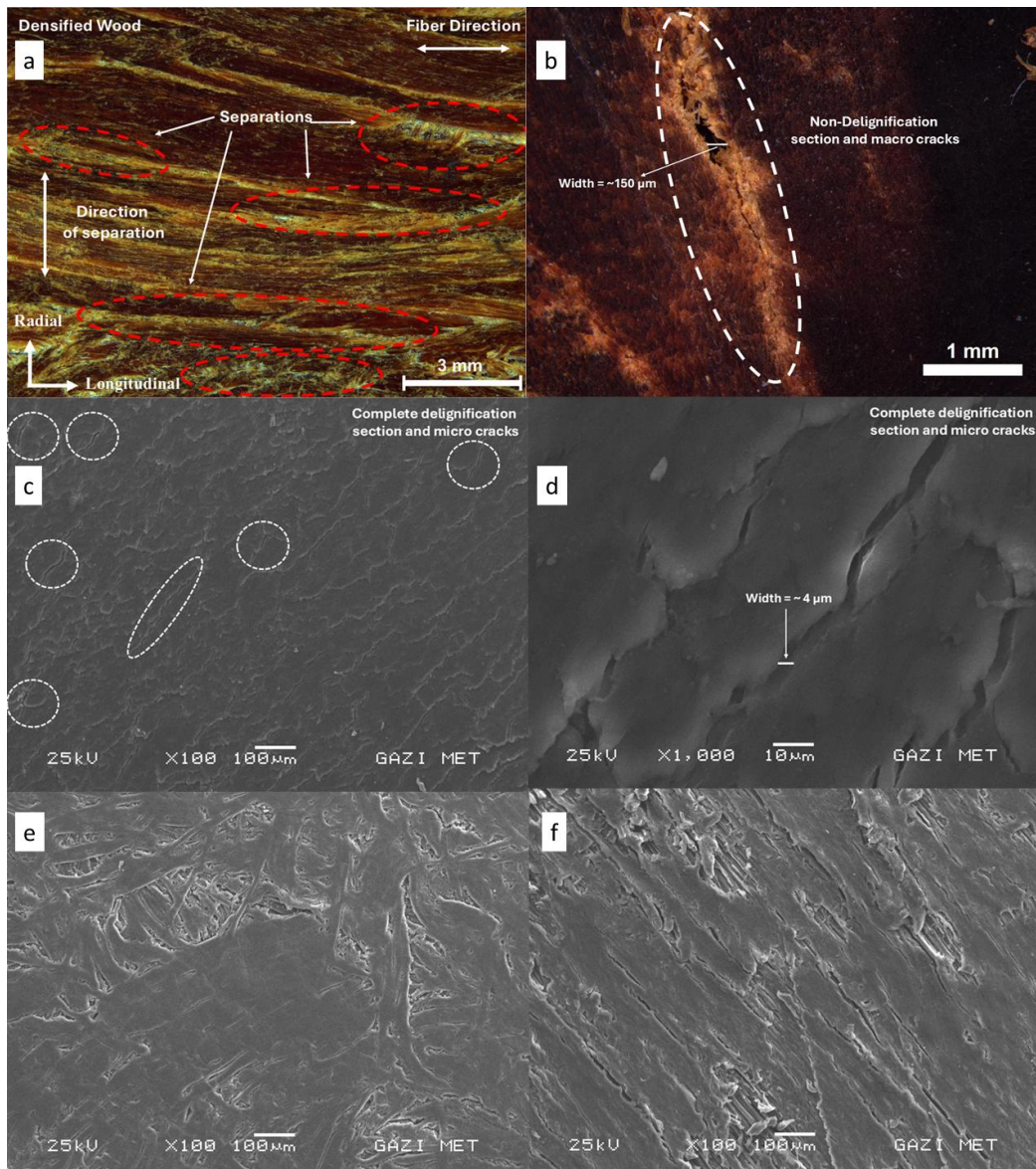


Fig. 4: Densified poplar on the stereo microscope: tangential (a), cross section (b). Densified poplar on SEM: cross section (c) and (d), tangential section (e), radial section (f).

The stress mismatch between the densified outer shell and the rigid, unbonded core resulted in severe separation, manifesting as macro-cracks with widths up to 150  $\mu\text{m}$  (Fig. 4b). This confirms that the macro-cracks are a direct result of heterogeneous chemical treatment and lack of bonding. However, the macro-cracks ( $\sim 150 \mu\text{m}$ ) identified in the core region during microscopic analysis reveal a critical 'scaling effect' regarding the adaptation of standard literature protocols to industrial dimensions. It was observed that the passive immersion method, although successful in prior literature, resulted in inadequate core softening for the 35 mm thick lumber used in this study. These structural discontinuities, resulting from the insufficient chemical softening of core fibres, experimentally confirm that the industrial upscaling of delignification-based densification requires more aggressive impregnation kinetics, such as vacuum-pressure impregnation. The diffusion limitation was further evidenced by the visual distinctness of the core region. As seen in Fig. 4b, the core retained the lighter,

natural colour of unmodified wood, contrasting with the darker, chemically modified shell. This indicates that the lignin matrix in the centre remained below its glass transition temperature ( $T_g$ ) during pressing, preventing the necessary plastic flow and causing brittle failure (macro-cracks) under the shear stress of the densified shell.

### **Unconstrained pressing and micro-cracks (~4 $\mu\text{m}$ )**

In contrast to the core defects, SEM analysis of the densified regions (Figs. 4c,d) revealed a network of numerous micro-cracks approximately 4  $\mu\text{m}$  in width. These micro-cracks are attributed specifically to the unconstrained pressing configuration. As the material was compressed radially, it underwent lateral expansion (Poisson effect) in the tangential direction. Without a mould to counteract this expansion, high tensile and shear stresses are concentrated at the ray parenchyma and cell wall interfaces, causing micro-fissures. This finding confirms that even in well-delignified regions, the lack of lateral confinement compromises the micro-structural integrity. The widespread micro-cracks (~4  $\mu\text{m}$ ) observed in the shell layer (Fig. 4d) align with the expected stress distribution in unconstrained compression. As the material was compressed radially, the induced tangential tensile stresses exceeded the transverse bonding strength of the delignified cell walls, leading to debonding at the ray parenchyma interfaces. This confirms that lateral confinement is not merely a shaping requirement but a structural necessity to counteract Poisson expansion in chemically modified wood. Without a mould to counteract this expansion, high tensile and shear stresses are concentrated at the ray parenchyma and cell wall interfaces, causing micro-fissures (Sandberg et al. 2017). This finding confirms that even in well-delignified regions, the lack of lateral confinement compromises the micro-structural integrity.

## **CONCLUSIONS**

This study characterized the effects of partial delignification followed by unconstrained hot pressing on poplar wood: (1) Mechanical transformation: Despite the lack of confinement, the process achieved a 172,6% increase in density, a 346.3% increase in hardness, a 67.4% increase in bending strength (MOR), and a 78.3% increase in MOE, proving the efficacy of the chemical pretreatment in facilitating densification and consolidating the cellulose network. (2) Macro-defect mechanism (core): A critical limitation was identified: Diffusion limitation of the chemical solution prevented delignification in the core. Consequently, the absence of effective hydrogen bonding in the core region induced the formation of macro-cracks up to 150  $\mu\text{m}$  during compression. This result experimentally verifies that while the standard delignification protocols in the literature are successful at the laboratory scale, they cannot be linearly upscaled to industrial lumber dimensions without modifying the impregnation kinetics. (3) Micro-defect mechanism (general): The absence of lateral confinement (unconstrained pressing) caused Poisson-induced lateral expansion, resulting in pervasive 4  $\mu\text{m}$  micro-cracks throughout the matrix. (4) Scientific implication: This study demonstrates that achieving high mechanical performance, such as stiffness and surface hardness, does not inherently guarantee structural integrity in bulk timber densification. To achieve a viable industrial product, future research

must address impregnation homogeneity (to eliminate core cracks) and utilize lateral confinement or secondary stabilization (to eliminate micro-cracks).

This study mechanistically demonstrates that chemical modification alone is insufficient to produce high-performance densified wood; achieving industrial viability under unconstrained conditions necessitates both homogeneous impregnation and lateral stabilization. Ultimately, this work serves as a structural benchmark, demonstrating that standard passive chemical modification strategies cannot be directly transferred to 35 mm thick poplar lumber densification without causing critical integrity losses due to diffusion limitations. This study proves that chemical modification alone is not sufficient for bulk timber. Future industrial applications must utilize vacuum-pressure impregnation (for core treatment) and active lateral confinement (to prevent micro-cracks).

Finally, regarding the scale effect: We intentionally applied the standard protocol to 35 mm thick lumber to experimentally demonstrate the critical diffusion limits (core macro-cracks) and the necessity of lateral confinement (near-surface micro-cracks) that are often overlooked in idealized laboratory studies. The mechanical values reported in this study were obtained from small, clear specimens extracted from the densified regions near the surface to allow comparison with existing literature (Song et al. 2018). These values represent the intrinsic potential of the modified regions. Achieving these high strengths homogeneously in full-sized structural elements cannot be realized through passive immersion or unconstrained pressing; it strictly requires industrial interventions such as vacuum-pressure impregnation and active lateral confinement.

### ACKNOWLEDGMENTS

This work was supported by the Gazi University Scientific Research Projects Coordination Unit under project number FLO-2022-7548.

### REFERENCES

1. Balatnecz, J.J. & Kretschmann, D.E. (2001): Properties and utilization of poplar wood. In: *Poplar Culture in North America, Part A, Chapter 9*, NRC Research Press, Ottawa, 277-291 pp.
2. Chen, C., Kuang, Y., Zhu, S., Burgert, I., Keplinger, T., Gong, A., ... & Hu, L. (2020). Structure–property–function relationships of natural and engineered wood. *Nature Reviews Materials*, 5(9), 642-666.
3. Frey, M., Schneider, L., Masania, K., Keplinger, T., & Burgert, I. (2019). Delignified wood–polymer interpenetrating composites exceeding the rule of mixtures. *ACS applied materials & interfaces*, 11(38), 35305-35311.
4. Bodig, J., & Jayne, B. A. (1982). *Mechanics of wood and wood composites* 61-62 pp.
5. Kutnar, A. & Kamke, F.A. (2012): Compression of wood under saturated steam conditions: mechanical response. In: *Wood Science and Technology* 46 (1-3), 75–88 pp.

6. Laine, K., Segerholm, K., Wälinder, M., Rautkari, L., & Hughes, M. (2016). Wood densification and thermal modification: hardness, set-recovery and micromorphology. *Wood science and technology*, 50(5), 883-894.
7. Yoshihara, H., & Nobusue, K. (2008). Mode I and mode II fracture toughness of densified Sitka spruce fabricated in an airtight atmosphere with high-temperature steam.
8. Morsing N (2000) Densification of wood - the influence of hygrothermal treatment on compression of beech perpendicular to the grain. Department of structural engineering and materials technical university of Denmark, Series R, 79, 138 pp.
9. Navi, P., & Heger, F. (2004). Combined densification and thermo-hydro-mechanical processing of wood. *MRS bulletin*, 29(5), 332-336.
10. Navi, P. & Sandberg, D. (2012): Thermo-hydro-mechanical wood processing. In: EPFL Press, Lausanne, 280 pp.
11. Rautkari, L., Properzi, M., Pichelin, F., & Hughes, M. (2009). Surface modification of wood using friction. *Wood Science and Technology*, 43(3), 291-299.
12. Sandberg, D., Haller, P., & Navi, P. (2013). Thermo-hydro and thermo-hydro-mechanical wood processing: An opportunity for future environmentally friendly wood products. *Wood Material Science & Engineering*, 8(1), 64-88.
13. Song, J., Chen, C., Zhu, S., Zhu, M., Dai, J., Ray, U., Li, Y., Kuang, Y., Li, Y., Li, H. V., Han, X. & Hu, L. (2018): Processing bulk natural wood into a high-performance structural material. In: *Nature* 554 (7691), 224–228 pp.
14. Tenorio, C., & Moya, R. (2021). Development of a thermo-hydro-mechanical device for wood densification adaptable to universal testing machines and its evaluation in a tropical species. *Journal of Testing and Evaluation*, 49(4), 2597-2608.
15. Wang, J., Fishwild, S. J., Begel, M., & Zhu, J. Y. (2020). Properties of densified poplar wood through partial delignification with alkali and acid pretreatment. *Journal of Materials Science*, 55(29), 14664-14676.
16. Zhu, M., Li, T., Davis, C. S., Yao, Y., Dai, J., Wang, Y., ... & Hu, L. (2016). Transparent and haze wood composites for highly efficient broadband light management in solar cells. *Nano Energy*, 26, 332-339.
17. Sandberg, D., Kutnar, A., & Mantanis, G. (2017). Wood modification technologies- A review. *Iforest-Biogeosciences and Forestry*, 10(6), 895.
18. Cheng, A., Tu, D., Zhu, Z., Zhou, Q., Wei, W., Hu, C., & Liu, X. (2022). Study on machining properties and surface coating properties of heat-treated densified poplar wood. *Wood Research*, 67(6), 1032–1045.
19. Chu, D., Li, X., Zhang, Y., & Mu, J. (2023). Effects of delignification level on the bending properties and failure mechanism of densified wood. *Forests*, 14(9), 1721.
20. Laine, K., Rautkari, L., Hughes, M., & Kutnar, A. (2016). Reducing the set-recovery of surface densified solid wood by furfuryl alcohol modification. *Journal Of Wood Science*, 62(3), 225–231.
21. Li, R., He, M., Liang, S., & Li, Z. (2021). Mechanical properties and engineering application potential of the densified poplar. *Construction And Building Materials*, 289, 123168.

22. Bytner, O., Laskowska, A., Drożdżek, M., Kozakiewicz, P., & Zawadzki, J. (2021). Evaluation of the dimensional stability of black poplar wood modified thermally in nitrogen atmosphere. *Materials*, 14(6), 1491.
23. Ülker, O., & Burdurlu, E. (2016). Some mechanical properties of densified and laminated lombardy poplar (*Populus nigra* L.). *Wood Research*, 61(6), 959–970.
24. Wang, Z., Gao, Z., & Wang, H. (2021). An optional connection material in timber structures: Densified poplar. *Bioresources*, 16(2), 3567–3581.
25. Zhou, Q., Liang, D., Cheng, A., Wang, X., & Tu, D. (2023). Effects of pressing temperature and compression ratio on density distribution and hardness of surface densified poplar wood. *Wood Research*, 68(3), 465–476.
26. Kuai, B., Wang, Z., Gao, J., Tong, J., Zhan, T., Zhang, Y., Lu, J., & Cai, L. (2022). Development of densified wood with high strength and excellent dimensional stability by impregnating delignified poplar by sodium silicate. *Construction And Building Materials*, 344, 128282.
27. Lykidis, C., Kotrotsiou, K., & Tsihlakis, A. (2020). Reducing set-recovery of compressively densified poplar wood by impregnation-modification with melamine-formaldehyde resin. *Wood Material Science & Engineering*, 15(5), 269–277.
28. Yu, Y., Zhang, F., Zhu, S., & Li, H. (2017). Effects of high-pressure treatment on poplar wood: Density profile, mechanical properties, strength potential index, And Microstructure. *Bioresources*, 12(3), 6283–6297.
29. Pelit, H., Budakçi, M., & Sönmez, A. (2018). Density and some mechanical properties of densified and heat post-treated Uludağ fir, linden and black poplar woods. *European Journal of Wood and Wood Products*, 76(1), 79-87.
30. Zhou, Q., Chen, C., Tu, D., Zhu, Z., & Li, K. (2019). Surface densification of poplar solid wood: Effects of the process parameters on the density profile and hardness. *Bioresources*, 14(2), 4814-4831.

ABDÜLHALİM BEŞPARMAK\*, HASAN ÖZGÜR İMİRZİ\*  
GAZI UNIVERSITY  
FACULTY OF TECHNOLOGY  
DEPARTMENT OF WOOD PRODUCTS INDUSTRIAL ENGINEERING  
06560 ANKARA  
TÜRKİYE

\*Corresponding authors: email: [abdulhalim.besparmak@gazi.edu.tr](mailto:abdulhalim.besparmak@gazi.edu.tr), [himirzi@gazi.edu.tr](mailto:himirzi@gazi.edu.tr)